Geomechanics and Engineering, *Vol. 22, No. 6 (2020) 529-540*
DOI: https://doi.org/10.12989/gae.2020.22.6.529

Modelling the coupled fracture propagation and fluid flow in jointed rock mass using FRACOD

Shichuan Zhang[1a], Baotang Shen[1,2b], Xinguo Zhang[*1], Yangyang Li[1c], Wenbin Sun[1d] and Jinhai Zhao[1e]

[1]*State Key Laboratory of Mining Disaster Prevention and Control, Shandong University of Science and Technology, Qingdao, China*
[2]*CSIRO Energy, Queensland Centre for Advanced Technologies, PO Box 883, Kenmore, Brisbane, QLD 4069, Australia*

(Received March 27, 2019, Revised August 5, 2020, Accepted August 18, 2020)

Abstract. Water inrush is a major hazard for mining and excavation in deep coal seams or rock masses. It can be attributed to the coalescence of rock fractures in rock mass due to the interaction of fractures, hydraulic flow and stress field. One of the key technical challenges is to understand the course and mechanism of fluid flows in rock joint networks and fracture propagation and hence to take measures to prevent the formation of water inrush channels caused by possible rock fracturing. Several case observations of fluid flowing in rock joint networks and coupled fracture propagation in underground coal roadways are shown in this paper. A number of numerical simulations were done using the recently developed flow coupling function in FRACOD which simulates explicitly the fracture initiation and propagation process. The study has demonstrated that the shortest path between the inlet and outlet in joint networks will become a larger fluid flow channel and those fractures nearest to the water source and the working faces become the main channel of water inrush. The fractures deeper into the rib are mostly caused by shearing, and slipping fractures coalesce with the joint, which connects the water source and eventually forming a water inrush channel.

Keywords: jointed rock; numerical simulation; fracture interaction; water inrush; FRACOD

1. Introduction

Mine water disaster is one of natural calamities which often happens in coal mine exploitations. It is the second largest mine disaster and threatens in the normal production of mine and the life of personnel seriously and has come into being a huge economic loss in China (Zhang *et al*. 2017, Zhou *et al*. 2015). Several water inrush accidents have been reported recently: (1) In November 2018, the return air inclined shaft at the -950m level of the Wanfu coal mine experienced a sudden increase in water inflow (SBCMES 2019). Water inrush occurred at the bottom and the average rate of inrushing water reached 14580 m^3/h. Because the quantity of maximum inrushing water was far greater than the drainage capacity of the mine, the inrush of sand and slurry became serious. This water inrush accident ultimately led to a loss of 1 live and a direct economic loss up to RMB 7.97 million (US $1.18 million). Based on the detailed geological prospecting work conducted, it is believed that the water inrush channel is formed by the fractures (joints) connected to the water conducted structure. The source of water irruption comes from the water aquifer of the Neogene. (2) In September 2003, water inrush occurred in the 10111 mining face of the Huangcun coal mine (Yu and Xing 2014). A large volume of ground water burst out. The water disaster has left 16 people dead and a direct economic loss up to RMB 56 million (US $8.35 million). The cause of the accident is the activation of concealed structures to conduct fracture propagation, which connect the floor limestone aquifer. Water inrush, caused by fracture propagation and coalescence (Saberhosseini *et al*. 2014, Tian and Yang 2017), threatens coal mine safety, and causes tremendous loss of life and property during mining. Therefore, understanding the course and mechanism of fluid flows in rock joint networks and fracture propagation is very important to predict water inrush in underground coal mine.

As the depth of mining and civil underground construction increases (Zhang *et al*. 2019a), coal extraction causes stress-induced rock fracturing inevitable, which may enhance hydraulic conductivity in the surrounding rock (Li *et al*. 2015, Wu *et al*. 2018). Meanwhile, the threat of water inrush disasters caused by water flowing fracture propagation is growing in intensity due to the complexity of the geological conditions, as shown in Fig.1. Quite often geological defects exist in the structural plane (Sun *et al*. 2016), and it is the initial damage, damage evolution and fracture propagation that result in various failure types of jointed rock. The existence of joints in the rock mass

∗Corresponding author, Professor
E-mail: Zhangxg@sdust.edu.cn
[a]Ph.D.
E-mail: 3732600186@qq.com
[b]Professor
E-mail: baotang.shen@csiro.au
[c]Ph.D.
E-mail: 996457633@qq.com
[d]Professor
E-mail: swb@sdust.edu.cn
[e]Ph.D.
E-mail: 363722411@qq.com

ISSN: 2005-307X (Print), 2092-6219 (Online)

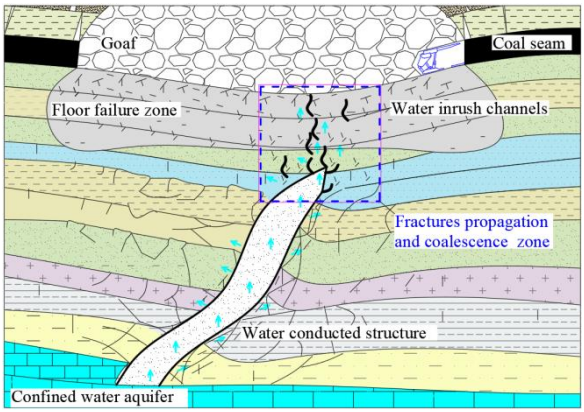

Fig. 1 Water inrush disaster due to fractures propagation in jointed rocks. Those water inrush channels are formed by the fractures connected with the water conducted structure, which connect the confined water aquifer

increase the level of water-rock contact and provides conditions for the formation of water inrush channels (Shen *et al*. 2015). Therefore, the study of the distribution characteristics of fluid flow and the mechanism of fracture propagation in the jointed rock is of importance for preventing coal water inrush (Dang *et al*. 2017). Lots of scholars and engineers have extensively studied the mechanism of water inrush (Chen *et al*. 2020), and their achievements play an important role in the prevention of water inrush disaster.

Men *et al*. (2018) performed a series of simulations by using the Rock Failure Process Analysis (RFPA) to understand the fracture propagation behavior of jointed rocks in hydraulic fracturing, and three basic kinds of hydraulic fractures of jointed rock are considered. Zhao *et al*. (2018) construct four typical joint system models separately comprising orthogonal, staggered, diagonal and randomly oriented joints and conducted the virtual hydraulic fracturing simulations by using the Universal Distinct Element Code (UDEC). McClure *et al*. (2016) developed a hydraulic-fracturing simulator that implicitly couples fluid flow with the stresses induced by fracture deformation in large, complex, 3D discrete-fracture networks (DFNs). It can describe propagation of hydraulic fractures and opening and shearing stimulation of natural fractures. So, several different types of "Continuum Numerical Methods" (CNM) have been used or developed for understanding the hydraulic fracturing (Shen and Barton 2018). Most existing simulation software can model the behavior of jointed or fractured rock mass, but they do not consider the explicit fracture initiation and propagation, which is a dominant mechanism in rocks. The discontinuum methods take into account the presence of distinct discontinuities, it allows the discrete discontinuities to be incorporated into the displacement field.

FRACOD is designed to simulate rock failure processes caused by explicit fracture initiation and propagation in elastic rock, based on fracture mechanics principle and a boundary element method (Wang *et al*. 2020). Now it also includes complex coupling processes between the rock fracturing, heat transfer and hydraulic flow. Since its initial development in 1990s, FRACOD has been used in many application studies, including the well-known ÄSPÖ Hard Rock Laboratory's Pillar Spalling Experiments (APSE) in Sweden (2004), the DECOVALEX International Collaboration Project and the Mizunami Underground Research Laboratory (MIU) Investigations in Japan (Rinne and Shen 2004, 2007). Since 2007, the focus of FRACOD development has shifted to the coupling between rock fracturing, fluid flow and thermal processes. The coupling between rock fracturing and fluid flow was achieved using an explicit approach and it employs a time marching iteration scheme for both fluid flow and fracture propagation (Sun *et al*. 2018). The new function is capable of simulating fluid flow in complex fracture networks and fracture movement and propagation driven by fluid pressure.

In this paper, we present a brief theoretical background and then discuss work related to the development of fracture-hydraulic flow coupling in FRACOD. Single fracture fluid flow validation example has been first provided. We simulated and analyzed the fluid flow characteristics in rock joint networks, and fluid pressure and flow variation in different paths at different time were studied. Next, through the modelling roadway water inrush, the three parameters of joint distribution in the coal seam were studied, such as without joints, single direction joints and two direction joints. Compared with previous research, this paper conducts a detailed study on the distribution characteristics of fluid flow and the mechanism of water inrush caused by fracture propagation, as opposed to only studying the destruction of surrounding rock.

2. Theoretical background of FRACOD

The basic theories and various applications to engineering problems can be found in Shen *et al*. (2015), and Stephansson *et al*. (2008). FRACOD is a two-dimensional boundary element code which follows the boundary element method (BEM) principles. The code employs the displacement discontinuity method (DDM) to predict the explicit fracturing process, including the possibility of fracture initiation and possibility and the path of fracture propagation. A brief theoretical background relevant to this paper is introduced below.

2.1 F-criterion

Tensile and shear failure are common in rock masses. When simulating fracture process, it is needed to consider mode I (tension), mode II (shear) and mixed mode I + II propagation. There are two major approaches for predicting fracture propagation: the principal stress/strain based criteria and the energy based criteria. The second approach includes the Maximum Strain Energy Release Rate Criterion (G-criterion) (Hou *et al*. 2019) and the Minimum Strain Energy Density Criterion (S-criterion) (Aliha 2019). However, G-criterion and S-criterion in their original form are not directly suitable for predicting both mode I and mode II fractures. Consequently, the original G-criterion had been improved and extended by Shen and Stephansson to form a new criterion (Shen and Stephansson 1994), the F-criterion. The F-criterion considers the individual contributions of tensile and shear fracturing in the total energy release rate, and measures them against the critical strain energy release rates due to both mechanisms, and hence be able to predict realistically the fracturing due to both tension and shear. The principle of the F-criterion can be stated as follows:

In an arbitrary direction (θ) at a fracture tip, $F(\theta)$ is defined by

$$F(\theta)=\frac{G_I(\theta)}{G_{Ic}}+\frac{G_{II}(\theta)}{G_{IIc}} \tag{1}$$

where G_{Ic} and G_{IIc} are the critical strain energy release rates for mode I and mode II fracture growth; G_I and G_{II} are strain energy release rates due to the potential mode I and mode II fracture growth of a unit length.

These are calculated numerically with these steps: (1) compute the strain energy based on the original crack; (2) add a fictitious crack increment Δa in direction θ, and compute the strain energies separately for the crack growth mode I and II based on this new fictitious crack; (3) divide the difference between the new and original strain energies by the incremental length Δa to obtain the approximate values of $G_I(\theta)$ and $G_{II}(\theta)$. Let $F(\theta)$ reach the maximum value $F_{\max}$ at $\theta=\theta_0$. The F-Criterion states that if $F_{\max}\geq 1$, fracture propagation will occur in the direction θ_0.

2.2 Fracture-hydraulic flow coupling

There are two fundamental approaches in modelling the coupled fracturing-hydraulic flow (F-H) processes in fractured rock. One is the implicit approach and the other is the explicit. In the first approach, related fluid flow equations, such as Darcy's law, are solved together with mechanical equations for rock medium. In the second approaches, however, both fluid flow and mechanical response are simulated by using a time marching iteration process. There are several well-known commercial codes, such as UDEC and 3DEC (Israelsson 1996), that are based on the explicit process.

The F-H coupling process in FRACOD is an explicit approach, and it uses the Displacement Discontinuity (DD) (Crouch 1976) method with an iteration process to simulate

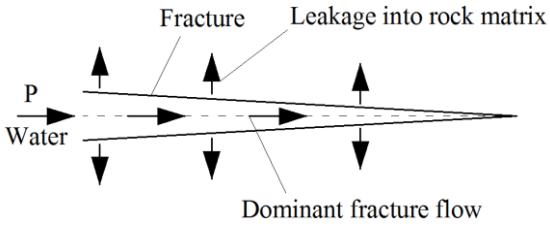

Fig. 2 Water paths of dominant fracture flow and minor leakage into rock matrix. P is water pressure

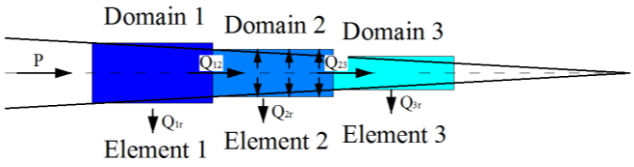

Fig. 3 Domain division for fluid flow simulation. Q_{ij}, the flow rate from Domain i to Domain j; Q_{ir}, the flow rate from Domain i to rock matrix

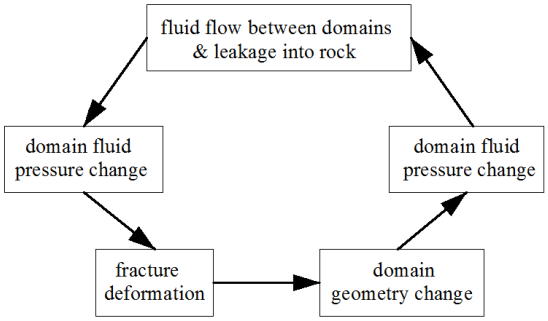

Fig. 4 A coupled F-H process

rock deformation and fracture propagation. In parallel it also uses the Cubic law combined with an iteration process to model the fluid flow processes in fractures. Comparing with the implicit approach, both the mechanical and fluid flow calculations with this explicit approach are mathematically simple to adopt complicated boundary conditions and changing model conditions. But it often needs longer computational time for flow solution.

2.2.1 basic model for fracture flow

In general, there are two ways of water inrush in mining face: water not only flows in the fracture channels but also leakages from the fracture channels to the surrounding intact rock. The paper considers both the flow in fractures and the leakage in intact rock, as shown in Fig. 2. The path of water inrush is dominantly the fracture channels, so-called "channels" water inrush or fracture water inrush, and in the rock it is seepage water inrush (Zhang *et al.* 2019b, Shen *et al.* 2020).

During the mechanical simulation using DD method, a fracture is discretized into a number of DD elements, as shown in Fig 3. In the flow calculation, each DD element is considered as a hydraulic domain and the adjacent domains are connected hydraulically. Fluid may flow from one domain to another depending on the pressure difference between the two domains.

2.2.2 Iteration scheme

A coupled F-H processes illustrated in Fig. 4, and the iteration steps are described below.

Step 1. Water flow occurs between fracture domains and water leaks into rock matrix. The water flow between fracture domains is calculated using the Cubic Law, that is, the flow rate between two adjacent domains is calculated using Eq. (2):

$$\mathrm{Q}=\frac{\mathrm{e}^3}{12\mu}\frac{\Delta P}{l} \tag{2}$$

where e is fracture aperture; l is domain length; ΔP is fluid pressure difference between the two domains; μ is dynamic fluid viscosity.

In fractured hard rock, the leakage is often much less significant than fracture channel flow. To simplify the simulation, we have adopted a simple approach to the fluid leakage process in this study. It is assumed that the fracture is effectively enclosed by a fictitious layer of intact rock of limited thickness at each surface side, and a constant fluid pressure (i.e. initial fluid pressure) exists on the outer boundary of the fictitious rock layer. The thickness of the fictitious layer represents the "effective" leakage distance. Obviously in the actual case the effective leakage distance may vary with time and location. But for simplicity, it is assumed that the effective leakage distance is fixed.

With the above assumption and simplifications, the flow leakage between a fracture domain and the surrounding intact rock is estimated using Eq. (3).

$$\mathrm{Q}_{\mathrm{leak}}=\frac{\mathrm{k}}{\mu}\frac{P-P_0}{d} \tag{3}$$

where k is permeability of rock; d is the effective leakage distance; P is domain fluid pressure; P_0 is initial pore pressure at the outer boundary of the fictitious rock layer.

Step 2. Water flow causes pressure changes in fracture domains. After small time duration Δt, the domain pressure will change as the water flow in or out a domain has changed the fluid volume. The new domain pressure is calculated using Eq. (4):

$$P\left(t+\Delta t\right)=P_0+K_w Q\frac{\Delta t}{V}-K_w Q_{leak}\frac{\Delta t}{V} \tag{4}$$

where K_w is fluid bulk modulus; V is domain volume; Δt is time step.

Step 3. Change in water pressure causes fracture deformation. The fracture domains are calculated using the DD method where the water pressures in fracture domains are the input boundary stresses. After considering the water pressure in the fracture domains (elements), the system of equations for calculation the element displacement discontinuities is given in Eq. (5).

$$\begin{cases}\left(\sigma_{\mathrm{s}}^{\mathrm{i}}\right)_0=\sum_{j=1}^{N}A_{ss}^{ij}D_s^i+\sum_{j=1}^{N}A_{sn}^{ij}D_n^i-K_s D_s^i\\ \left(\sigma_{\mathrm{n}}^{\mathrm{i}}\right)_0+P(t+\Delta t)-P_0=\sum_{j=1}^{N}A_{ns}^{ij}D_s^i+\sum_{j=1}^{N}A_{nn}^{ij}D_n^i-K_n D_n^i\end{cases} \tag{5}$$

where $(\sigma_s)_0$, $(\sigma_n)_0$ are the in-situ stresses in tangential and normal directions of the fracture surface; D_s, D_n are the displacement discontinuities in shear and normal directions; A_{ss}, A_{sn}, A_{ns}, A_{nn} are influence coefficients of the displacement discontinuity on the tractions on the fracture elements; K_s and K_n are fracture shear and normal stiffnesses.

Step 4. Fracture deformation changes the domain volume, and hence changes the water pressure in domains. The new domain pressure is calculated using Eq. (6)

$$P'\left(t+\Delta t\right)=P\left(t+\Delta t\right)-K_w\frac{\Delta \mathrm{e}\cdot l}{V} \tag{6}$$

where $P(t+\Delta t)$ is domain pressure before fracture deformation; $P'(t+\Delta t)$ is new domain pressure after fracture deformation; Δe is the change in fracture aperture.

The new domain fluid pressures are then used to calculate the flow rate between domains in Step 1. Steps 1 to 4 are iterated until the desired fluid time is reached and a stable solution is achieved.

3. Validation of fluid flow function

3.1 Single fracture fluid flow example case

A single fracture fluid flow example case has been modelled using the coupled F-H code of FRACOD. This case only tests the fluid flow function with mechanical coupling, hence the single fracture linking the two holes has a constant initial aperture 10um (Zhang *et al.* 2019b). Two boreholes are of a diameter of 1m, and are 20m apart. Left hole is the inlet hole and has a constant fluid pressure of 6 MPa, the right hole is the outlet hole and the fluid pressure are 0. The single fracture was set as the monitoring line to monitor the change characteristics of fluid pressure and flow rate at different times. The key mechanical and fracture properties used in simulated test are shown in Table 1.

3.2 Modeling results and discussions

The modelled fluid pressure distribution with time in the single fracture is shown in Fig. 5(a) and Fig. 6(a). The results demonstrate a dynamic process of fluid flow from the inlet hole to the outlet hole in 0.2s, 0.5s, 1.5s and 10s. Affected by the water pressure between two holes, the fluid flows from the inlet to the outlet. After 0.2s, 0.5s and 1.5s, the fluid pressure front travelled about 9m, but the pressure distribution is still nonlinear before 1.5s. After about 10s, the fluid flow in the single fracture has reached a steady state solution and the pressure is linearly distributed.

Table 1 Some input parameters for the validation case

Fracture toughness	Mode I/MPa·m$^{1/2}$	1.5	Rock	Young's modulus/*GPa*	37.5
	Mode II/ MPa·m$^{1/2}$	3.0		Poisson's ratio	0.25
Fluid	Bulk modulus/*GPa*	1.0		Internal friction angle/◦	33
	Density/*kg·m*$^{-3}$	1000		Cohesion/*MPa*	33
	Viscosity/ *Pa·s*	1.0×10^{-3}		Porosity	0.1

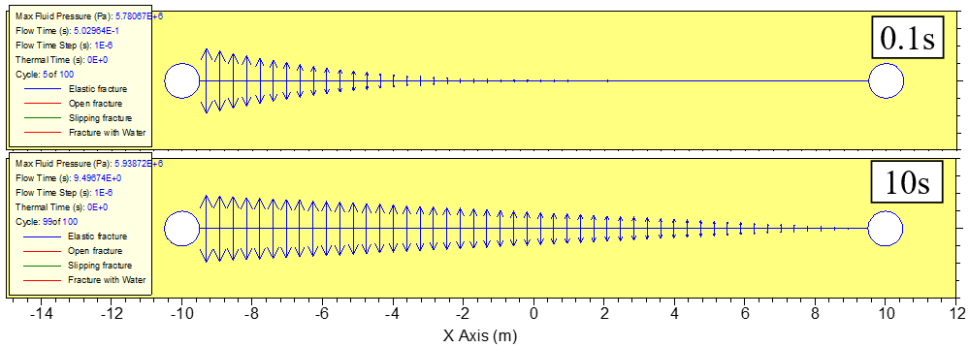

(a)

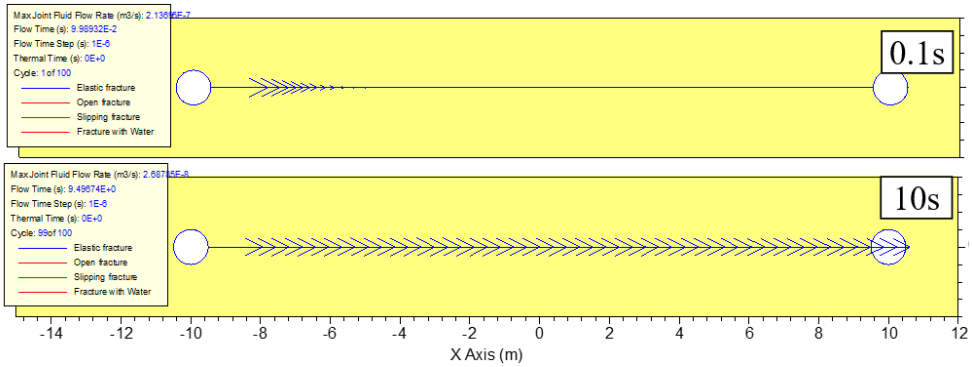

(b)

Fig. 5(a) fluid pressure distribution in single fracture at 0.1s and 10s and (b) Fracture fluid flow rate in single fracture at 0.1s and 10s

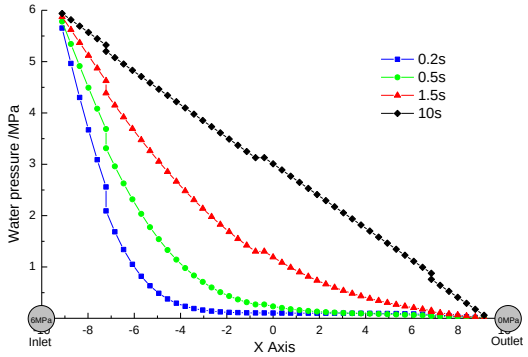

(a)

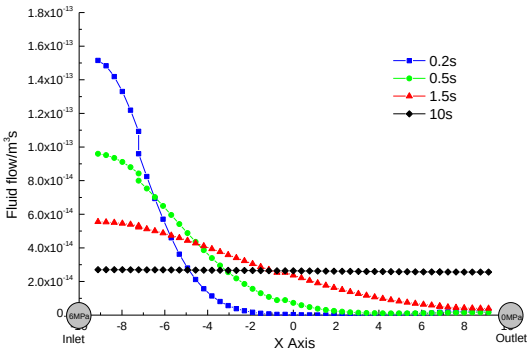

(b)

Fig. 6 Distribution characteristics of water pressure and flow

The modelled fluid flow distribution with time in the single fracture is shown in Fig. 5(b) and Fig. 6(b). In Fig. 5(b), the size and orientation of the arrow indicate the flow size and flow direction, it can be seen that the flow direction is consistent with the tangential direction of the single fracture. After about 10s, the fluid flow has reached a steady state and the flow is uniformly distributed. Before reaching the steady stage, the flow near the inlet is larger than that in other areas, and the flow gradually decreases with the distance increase from the inlet. The results of the tests show that the F-H code of FRACOD is working properly according to the expectation.

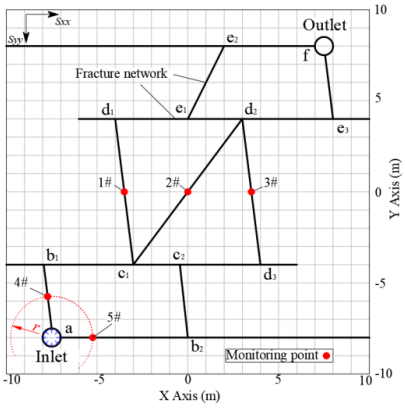

Fig. 7 Rock fracture network fluid flow test

4. Fluid flow characteristics in rock joint networks

The threat of water inrush, such as fluid flow in complex joint networks, is growing in intensity due to the increasing

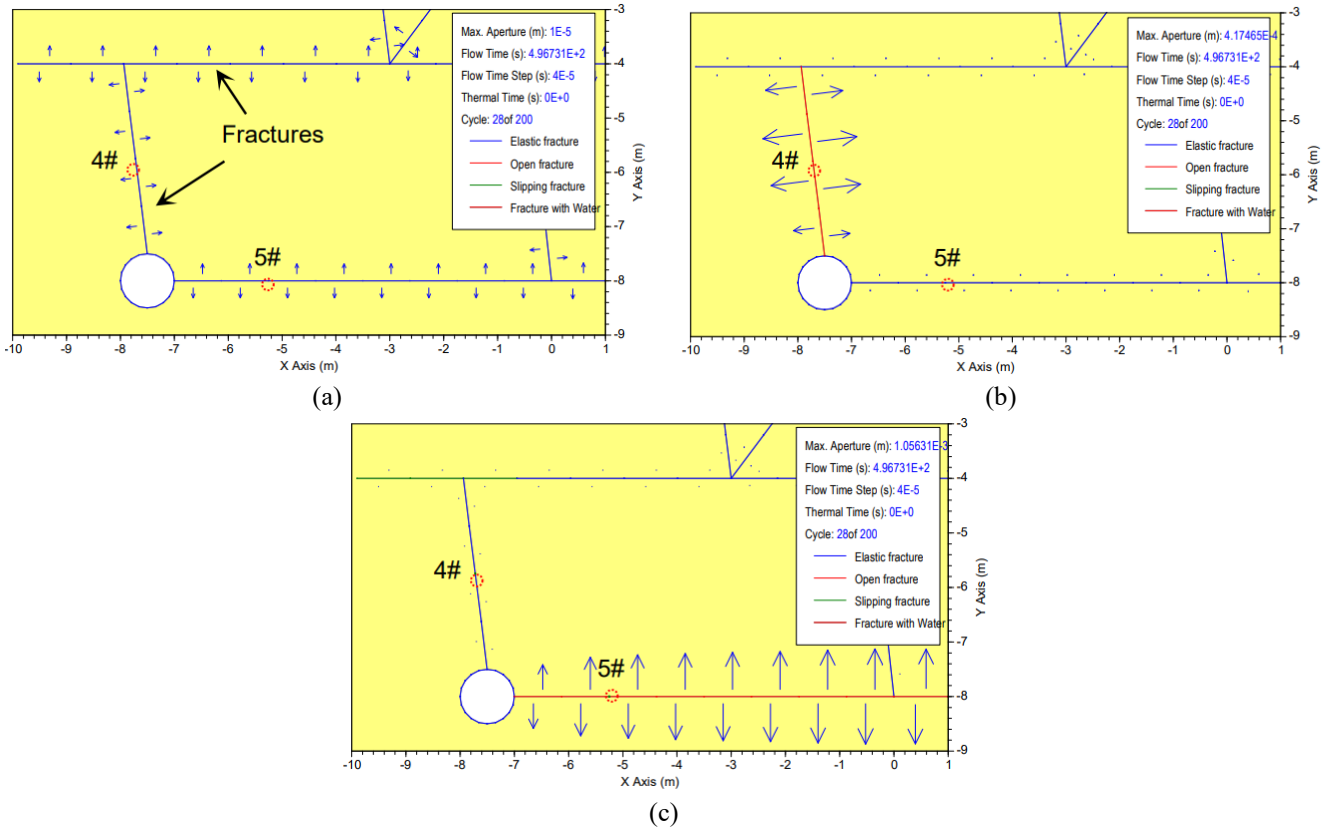

Fig. 8 Coupled solution of fracture dilation in 500s. Blue arrows on the pre-existing fractures represent the relative magnitude of the fracture aperture in Case 1 (a), Case 2 (b) and Case 3 (c)

depth and the complexity of the geological conditions in underground coal mines. Because of the existence of joints in the rock mass, it is complicated to analyze the stability of underground engineering. Therefore, the study of the distribution characteristics of the fluid flow path with time in the fracture networks is of importance for preventing coal water inrush.

4.1 Modeling fluid flow under different stress

In view of the actual geological conditions, fluid flow in joint networks is affected by in-situ stress, such as horizontal stress (σ_h) and vertical stress (σ_v), and the stress ratios $\sigma_h/\sigma_v \neq 0$. Two boreholes are considered in a rock mass linked by 11 intersecting fractures, whose initial aperture is 10um. Two boreholes are of a diameter of 1m, the fluid pressure in inlet hole is 6 MPa and the outlet is 0. To monitor the fluid flow characteristics of different flow path, five monitoring points (1#~5#) were designed, as shown in Fig. 7, and 4# and 5# are the same distance from the inlet. Some mechanical properties of rock and fluid and fracture properties used in simulation is shown in Table 1.

In this numerical study, three cases using different stress ratios as listed below were studied:

Case 1: The buried depth of the rock mass is about 400 m, the vertical pressure is 10 MPa.

Case 2: The buried depth of the rock mass is about 200 m, the vertical pressure is 10 MPa.

Case 3: The buried depth of the rock mass is about 400 m, the vertical stress is 5 MPa.

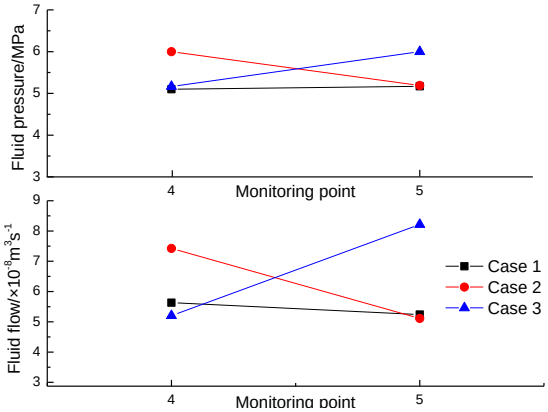

Fig. 9 Fluid flow and fluid pressure at monitoring points 4# and 5# at 500s

The purpose of Case 1 is to simulate the fluid flows in actual geological conditions. Case 2 and Case 3 are to investigate distribution characteristics in fluid flow path with different stress ratio.

4.2 Modeling results and discussions

In this test, the study simulated the coupled process in which fluid flow in the joint networks causes fracture sliding and dilation. Fracture dilation increases the fracture aperture and enhances the fluid flow, so fluid flow shows different flow characteristics at different time, paths and stress ratios.

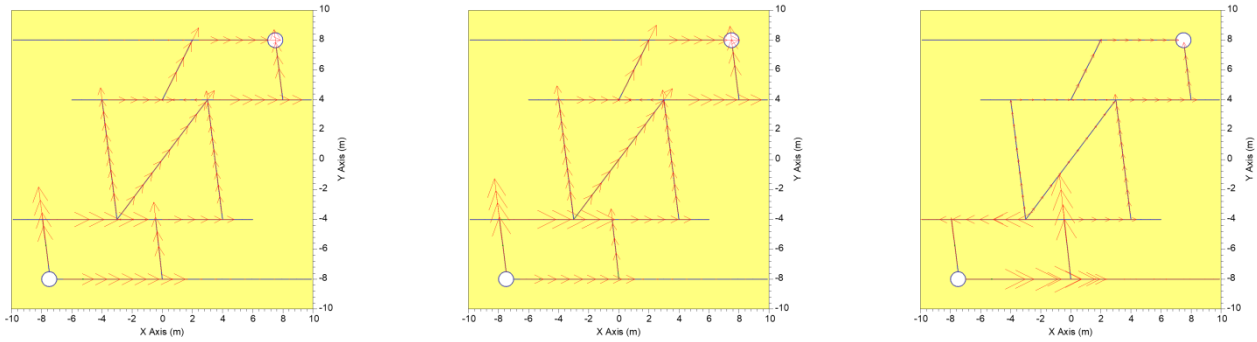

(a) (b) (c)

Fig. 10 Steady state solution of a coupled process involving fracture fluid flow in case 1 (a), case 2 (b) and case 3 (c)

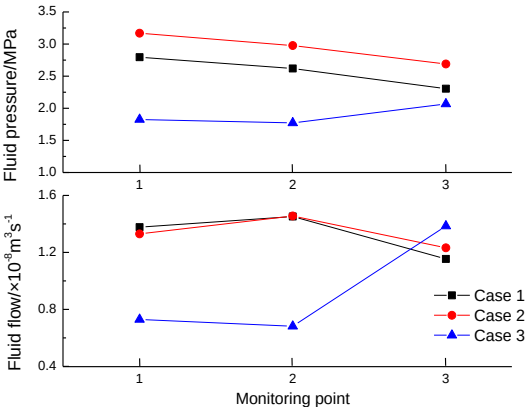

Fig. 11 Fluid flow and fluid pressure in monitoring points 1#,2# and 3# under the steady state.

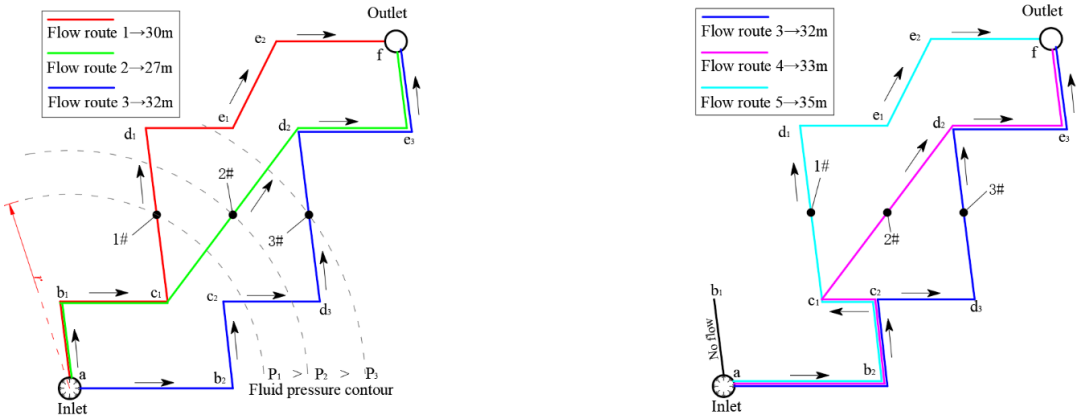

(a) (b)

Fig. 12 Characteristics of fluid flow in fracture networks under steady state. (a), three typical flow routes in case 1 and case 2 and (b), three typical flow routes in case 3

4.2.1 Fracture opening effect of in-site stress and fluid pressure

The modelled results of fracture aperture in 500s are shown in Fig. 8, different trends are observed for the predicted fracture dilation near inlet hole in three cases. In case 1 (σ_h/σ_v=1), the applied fluid pressure is relatively low and is predicted not to cause a fracture opening (Fig. 8(a)), and the fracture aperture is constant. However, the fluid pressure in the fractures is predicted to cause fluid flow toward the outlet hole. As shown in Fig. 9, the values of fluid pressure and fluid flow at monitoring points 4# and 5# are basic same in 500s.

Two additional simulations were conducted using the same model in case 2 and case 3. The modeling results are given in Fig. 8(b) and Fig. 8(c), the fracture opening appears in different directions because of different stress ratios. When σ_h/σ_v=0.5 (Case 2), the vertical fracture at the top of the inlet hole expanded obviously, it increased the fracture aperture and enhances the fluid flow. The values of fluid pressure and fluid flow at 4# are larger than that of 5# at this instant (Fig. 9) because of fracture opening.

When σ_h/σ_v=2 (Case 3), the horizontal fracture dilated and the vertical fracture aperture is constant, it causes the fluid pressure and fluid flow of 5# greater than 4# (Fig. 9).

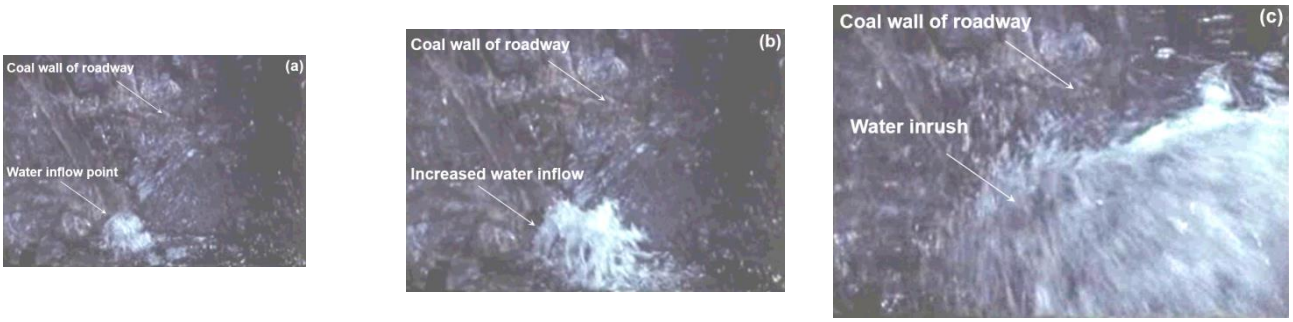

Fig. 13 A water inrush event at underground coal mine, China. The water burst out during roadway development.

The three examples demonstrate the significant effect of in-situ stress and fluid pressure on the movement of the pre-existing fractures in the rock mass, and the aperture change by fracture opening also enhances the fluid flow. The result shows that when the direction of the fracture is parallel to that of the greatest principal stress, the effect of in-situ stress on the fracture dilation is the biggest, and those fractures become the main channel of fluid flow.

4.2.2 Fluid flow characteristics at different paths

After 4000s, the fluid flow has reached a steady state solution, and water pressure is distributed at every position of the fracture networks. There is fluid flow in the fracture networks between the inlet and outlet, but the water flow in 1#, 2# and 3# positions is different due to the stress ratio, as shown in Fig. 10. When σ_h/σ_v=1 (Fig. 10(a)) and σ_h/σ_v=0.5 (Fig. 10(b)), the arrow in the middle fracture, through 2#, is bigger than those in other fractures, the flow in the middle fracture is the largest. When σ_h/σ_v=2, the arrow in the right fracture (3#) is bigger.

With the increase of fluid flow time, the fluid pressure and fluid flow in 1#~3# increase gradually and keep stable., There are differences in monitoring data under the steady state because of the different locations of the three monitoring points, as shown in Fig. 11. In case1 and case 2, the maximum values of fluid pressure and fluid flow are at 1# and 2# respectively. In case 3, the maximum values are at 3#.

In case 1 (Fig. 10(a)) and case 2 (Fig. 10(b)), no fracture was closed in the fracture networks under the steady state, so three typical flow routes were considered to study the characteristics of fluid flow in different fractures, as shown in Fig. 12a. Flow route 1: a→b1→c1→d1→e1→e2→f, flow distance is 30m, including 1#; Flow route 2: a→b1→c1→d2→e3→f, flow distance is 27m, including 2#; Flow route 3: a→b2→c2→d3→d2→e3→f, flow distance is 32 m, including 3#. It is noteworthy that there are many other routes for the fluid flow in the fracture networks, but they have little change in the flow distance, so we only consider the three routes.

Compared with case 3, there is no crack closure under the steady state in case 1 and case 2, so the water pressure and flow rate of the two cases are similar (Fig. 11). According to Fig. 11, the fluid pressure of three points is $P_1 > P_2 > P_3$ in case 1 and case 2, and the obvious contour distribution characteristics could be captured from (Fig. 12(a), dotted line). As the fluid flow is centered by the inlet, larger radius, therefore, corresponds to the lower fluid pressure. Meanwhile, the distribution characteristics of fluid flow are 2# > 1# > 3# under the steady state.

In case 3, the fracture of a-b_1 was closed and there is no fluid flow under the steady state (Fig. 10(c)), so there are two other typical flow routes, flow route 4 and flow route 5, as shown in Fig. 12(b). The water flow at 3# is much higher than at 1# and 2# (Fig. 12) within the figure 12b rout 3 has the shortest distance. The horizontal fracture of c_2-d_3 dilated, which causes the fracture aperture of c_3-d_2 (flow route) greater than c_1-d_2 and c_1-d_1 (flow route). Based on the change of fracture aperture and flow rate, the fluid pressure of 3# is higher than 1# and 2#. It can be seen from the simulated results that the shortest path will become a larger fluid flow channel when water flows in fractured network, and those fractures nearest to the inlet and outlet become the main channel of water inrush.

5. Modelling roadway water inrushes by fracture propagation in underground coal mines

Fig. 13 shows the Roadway water bursting event occurred at the underground coal mine in China, which resulted in lots of mine water pours out. The water in coal rib of an underground roadway gradually burst out during roadway development, caused by the gradual formation of water inrush channels. The mechanisms of water inrush in the rib with joints are unclear, but it is highly likely that fractures propagation and coalescence have occurred.

In this section, three additional models, one without joints and two with joints, have been used to simulate the fracture propagation, which connect water sources caused water inrush, around a roadway heading in an underground coal mine. The coal seam is at a depth of 800 m with in situ stresses $\sigma_{H\max}=\sigma_v$=19.6 MPa. It has a thickness of 3m, and roof and floor rocks are assumed to be massive siltstone units. The simulated roadway has a rectangular shape with a size of 4 m (width) and 3 m (height). The strength and fracture toughness of the rock and coal are shown in Table 2. Fracturing is considered in the coal seam and siltstone units in this case.

In order to study the water inrush issue in underground coal mines, a water source with high pressure (5 MPa) is assumed on the left side of roadway. Fractures without water bear the roadway face will propagate toward the direction of the water source after excavation. When those

Table 2 Some parameters for the modelling roadway case

	Young's modulus/GPa	Poisson's ratio	Tensile strength/MPa	Internal friction angle/°	Cohesion/MPa	Fracture toughness/MPa·m$^{1/2}$	
						Mode I	Mode II
Coal	2.0	0.25	0.1	41	2.3	1.0	0.3
Siltstone	20	0.25	2.2	35	9.5	6.7	1.5

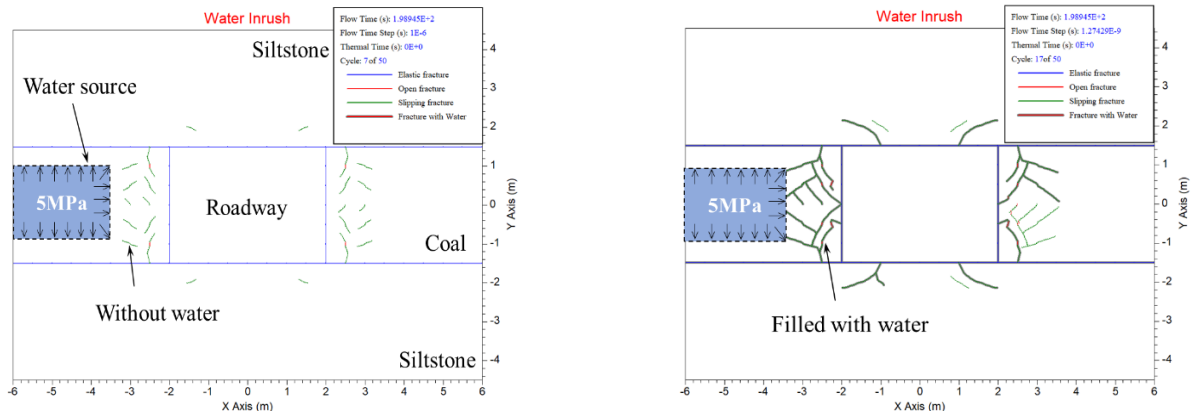

(a) (b)

Fig. 14 Predicted failure and water inrush in roadway ribs due to fracture initiation and propagation. (a) Early stage of the fracturing and (b) final stage of the water inrush

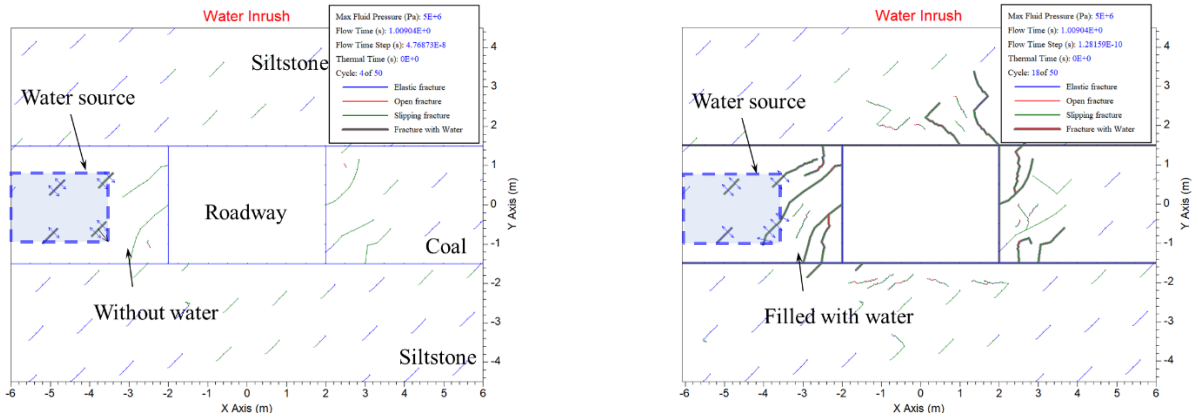

(a) (b)

Fig. 15 Predicted failure and water inrush in roadway ribs when single direction joints are considered. (a) early status with joints and (b) final stage of the water inrush

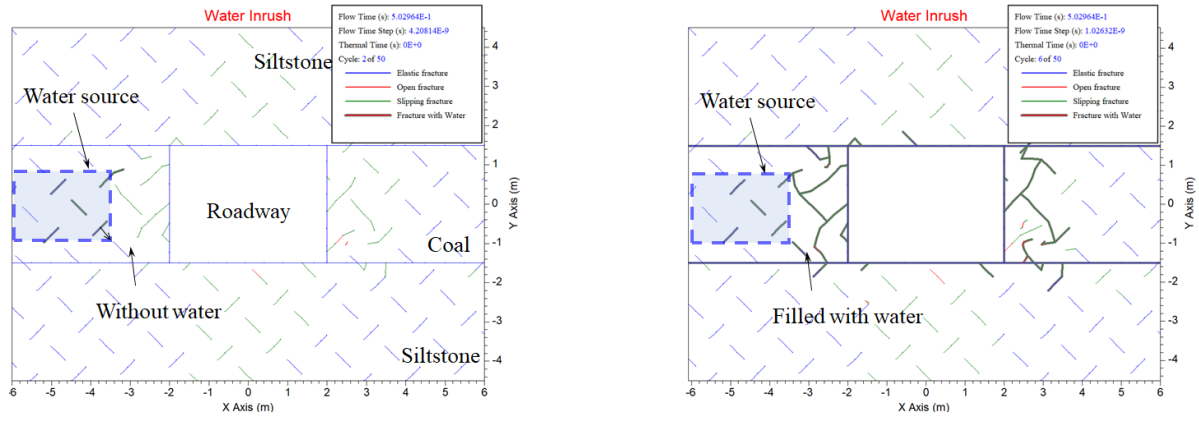

(a) (b)

Fig. 16 Predicted failure and water inrush when two direction short joints are considered. (a) early status with joints and (b) final stage of the water inrush

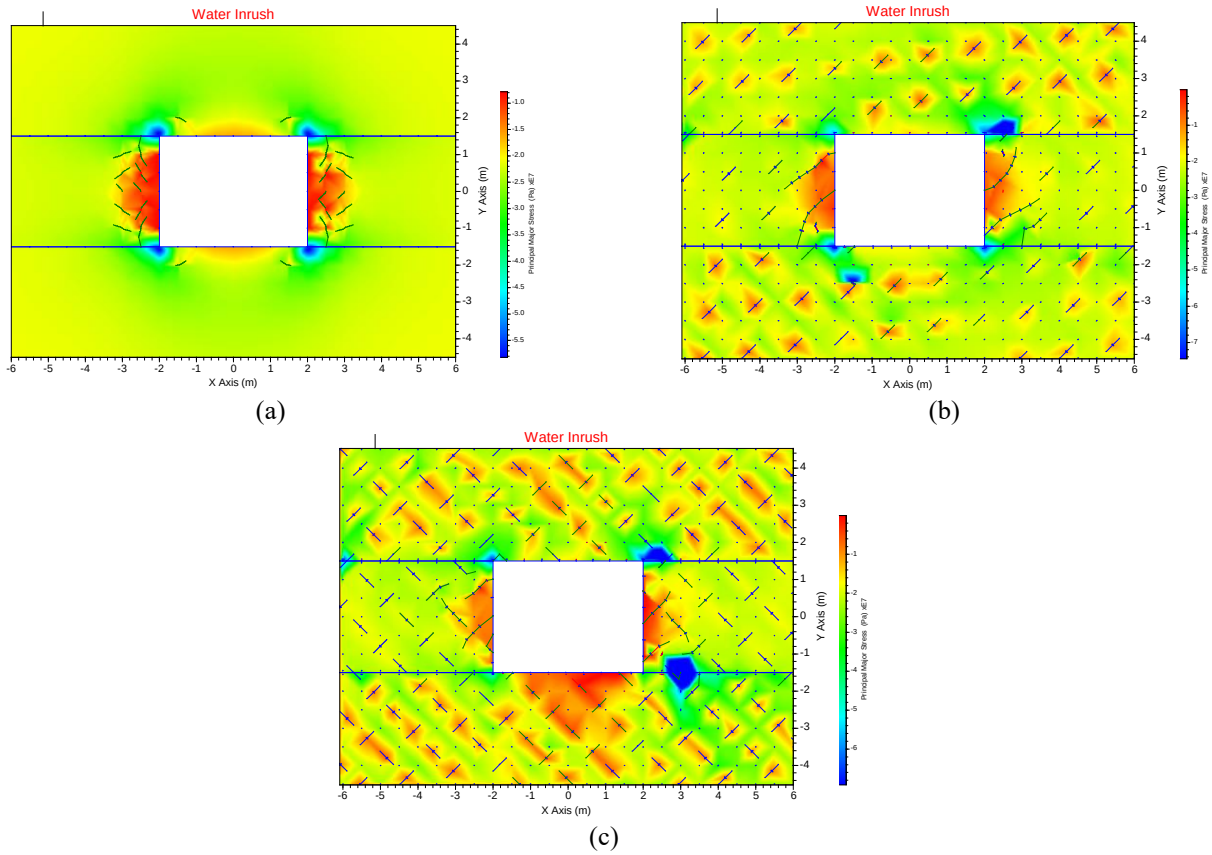

Fig. 17 Major principal stress distribution in the surrounding rock mass. (a) roadway model without joints, (b) model with single direction joints and (c) model with two direction joints

fractures coalesced with a water source, fractures will enhance water flow by creating new flow channels.

5.1 Pathway formation of water inrush channel caused by fracture propagation

5.1.1 Roadway without joints in the coal seam

This model was run without considering explicitly the joints in the coal seam. After the roadway excavation, short fractures parallel or at a small angle with the coal rib wall are formed (Fig. 14(a)). These short fractures are caused by tensile strain resulted from high compressive stress. The tensile strength of siltstone is much higher than coal, so fractures in siltstone seam are small in the size and few in number. The fracture however trend to propagate in shear and coalesce with each other to form larger fractures and develop progressively deep into the roadway ribs. Finally, those fractures propagated toward the direction of the water source, water inrush channels are formed and high-pressure water gushed into the roadway face after those fractures coalesced (Fig. 14(b)).

It is noticed that the shear fracture propagation and coalescence with water source in the failure region are the main causes of water inrush. Shear fractures are likely to be unstable, which could develop progressively deeper into the roadway surrounding rock.

5.1.2 Roadway with joints in the coal seam

The second model (Fig. 15) considers single direction joints in the coal seam and surrounding rock, the angle between joint and coal seam is 45°. The joints have a limited length and are set to propagate when the stress intensity factor reach the critical value. All others geometrical and mechanical parameters in the second and the third models (Fig. 16) are the same as in the first model. As shown in Fig. 15(a), the predicted failure in the ribs starts near the roadway wall mainly caused by the propagation and coalescence of the existing short joints. Joints near roadway become slipping fractures and they trend to propagate along the initial direction of the joints in Cycle 4. After Cycle 15(Fig. 15(b)), the slipping fractures expand deeper into the rib and coalesce with the joint, which connects the water source and has a high-water pressure inside, and eventually forming a water inrush channel. Some fracture initiations also occur further into the rib, but they do not coalesce with other joints and form any major failure. According to the test results, it is most easier to form water inrush channels as propagation and coalescence neighboring joints between roadway and high-pressure water source.

The third model considers two sets of short joints and orthogonal to each other (Fig. 16). Joints near roadway propagate along the initial direction of joints in Cycle 2 (Fig. 16(a)), and fast coalesce with other joints because the high-density distribution of the joints (Fig. 16(b)). Eventually, high-pressure water pours into the roadway along the joints.

The modelling indicates that joints in the surrounding

rock are playing a positive role in reducing the stress concentration and reducing the intensity and the extents of rock fracturing, but they provide favorable conditions for the formation of the water inrush channel. Consistent with the first model, it was observed that the fractures occurred are caused by mixed tensile and shear failures, but deeper into the rib the fracturing is mostly caused by shearing. So, it is conducive to fracture propagation to the depth of the rib if the joint is perpendicular to the roadway wall. Therefore, the initial direction of joints plays an important role in fracture propagation.

5.2 Stress distribution characteristics

FRACOD can also calculate the distribution of major principal stress. The effect of joints can further be demonstrated by examining the stress distribution in the surrounding rock mass, see Fig. 17. The stress in the vicinity of the roadway without joints are predominantly tensile stresses (Fig. 17(a)). The existence of joints in the surrounding rock mass has somewhat altered the tensile stress distribution because the joints can release the tensile stresses to some extent (Fig. 17(b)). When the joint density increases by 50% (Fig. 17(c)), the release degree of tensile stress is higher than that of single direction joints. The stress release and the change of tensile zone in the surrounding rock mass due to joints have important implications for the integrity of the roadway. With the increase of joint density, the distance between joints is shortened and fractures propagation and penetration are accelerated. Meanwhile, the permeability of the rock mass will be significantly increased and this provide conditions for the formation of water inrush channels.

6. Conclusions

Understanding the course and mechanism of fluid flow in rock joint networks and fracture propagation is very important to predict water inrush in underground coal mine. Three examples of modeling fluid flow under different stress in rock joint networks demonstrate that in-situ stress and fluid pressure have significant effects movement of fluid in pre-existing fractures in the rock mass, and the aperture change by fracture opening also enhances the fluid flow. When the direction of the fracture is parallel to that of the greatest principal stress, the effect of in-situ stress on the fracture dilation is the biggest, and those fractures become the main channel of fluid flow. Meanwhile, the shortest path will become a larger fluid flow channel when water flows in fractured network, and those fractures nearest to the water source and the underground working faces become the main channel of water inrush.

Based on three roadway models results, the fractures occurred at the rib are caused by mixed tensile and shear failures, but deeper into the rib the fracturing is mostly caused by shearing. The slipping fractures coalesce with the joint, which connects the water source and has a high-water pressure inside, and eventually form a water inrush channel. With the increase of joint density, the distance between joints is shortened and fractures propagation and penetration are accelerated, the permeability of the rock mass will be significantly increased and this provide conditions for the formation of water inrush channels.

References

Aliha, M.R.M. (2019), "On predicting mode II fracture toughness (K_{IIc}) of hot mix asphalt mixtures using the strain energy density criterion", *Theor. Appl. Fract. Mech.*, **99**, 36-43. https://doi.org/10.1016/j.tafmec.2018.11.001.

Chen, B., Zhang, S., Li, Y. and Li, J. (2020), "Experimental study on water and sand inrush of mining cracks in loose layers with different clay contents", *B. Eng. Geol. Environ.*, 1-16. https://doi.org/10.1007/s10064-020-01941-5.

Crouch, S.L. (1976), "Solution of plane elasticity problems by the displacement discontinuity method. I. Infinite body solution", *Int. J. Numer. Meth. Eng.*, **10**(2), 301-343. https://doi.org/10.1002/nme.1620100206.

Dang, W., Fruehwirt, T. and Konietzky, H. (2017), "Behaviour of a plane joint under horizontal cyclic shear loading", *Geomech. Eng.*, **13**(5), 809-823. https://doi.org/10.12989/gae.2017.13.5.809.

Hou, C., Jin, X., Fan, X., Xu, R. and Wang, Z. (2019), "A generalized maximum energy release rate criterion for mixed mode fracture analysis of brittle and quasi-brittle materials", *Theor. Appl. Fract. Mech.*, **100**, 78-85. https://doi.org/10.1016/j.tafmec.2018.12.015.

Israelsson, J.I. (1996), *Short Descriptions of UDEC and 3DEC*, in *Developments in Geotechnical Engineering*, Elsevier, 523-528.

Li, L.P., Lei, T., Li, S.C., Xu, Z.H., Xue, Y.G. and Shi, S.S. (2015), "Dynamic risk assessment of water inrush in tunnelling and software development", *Geomech. Eng.*, **9**(1), 57-81. https://doi.org/10.12989/gae.2015.9.1.057.

McClure, M.W., Babazadeh, M., Shiozawa, S. and Huang, J. (2016), "Fully coupled hydromechanical simulation of hydraulic fracturing in 3D discrete-fracture networks", *SPE J.*, **21**(4), 1-302. https://doi.org/10.2118/173354-PA.

Men, X., Li, J. and Han, Z. (2018), "Fracture propagation behavior of jointed rocks in hydraulic fracturing", *Adv. Mater. Sci. Eng.* https://doi.org/10.1155/2018/9461284.

Rinne, M. and Shen, B. (2007), "Numerical simulation of core tests using FRACOD in understanding and characterizing of the Excavation Disturbed Zone (EDZ)", DECOVALEX Task B Phase 2 Report, SKI Report, 8.

Rinne, M., Shen, B. and Lee, H.S. (2004), "Modelling of fracture development of APSE by FRACOD", Äspö Pillar Stability Experiment, The Swedish Nuclear Fuel and Waste Management Co.(SKB), Stockholm, Sweden.

Saberhosseini, S.E., Keshavarzi, R. and Ahangari, K. (2014), "A new geomechanical approach to investigate the role of in-situ stresses and pore pressure on hydraulic fracture pressure profile in vertical and horizontal oil wells", *Geomech. Eng.*, **7**(3), 233-246. http://doi.org/10.12989/gae.2014.7.3.233.

Shen B., Zhang B., Zhang S. and Chen B. (2020), "Application and verification of Fracod in rock engineering", *J. Shandong Univ. Sci. Technol. Nat. Sci.*, **39**(2), 44-52.

Shen, B. and Barton, N. (2018), "Rock fracturing mechanisms around underground openings", *Geomech. Eng.*, **16**(1), 35-47. https://doi.org/10.12989/gae.2018.16.1.035.

Shen, B. and Stephansson, O. (1994), "Modification of the G-criterion for crack propagation subjected to compression", *Eng. Fract. Mech.*, **47**(2), 177-189. https://doi.org/10.1016/0013-7944(94)90219-4.

Shen, B., Jung, Y.B., Park, E.S. and Kim, T.K. (2015), "Modelling the effect of ice swelling in the rock mass around an LNG

underground storage cavern using FRACOD", *Geosyst. Eng.*, **18**(4), 181-198. https://doi.org/10.1080/12269328.2015.1044575.

Stephansson, O., Shen, B., Rinne, M., Amemiya, K., Yamashi, R. and Toguri, S. (2008), "FRACOD modeling of rock fracturing and permeability change in excavation damaged zones", *Proceedings of the 12th International Conference of International Association for Computer Methods and Advances in Geomechanics (IACMAG)*, Goa, India, October.

Sun, W., Wang, X., Wang, L., Zhang, J. and Song, X. (2016), "Multidisciplinary design optimization of tunnel boring machine considering both structure and control parameters under complex geological conditions", *Struct. Multidisciplin. O.*, **54**(4), 1073-1092. https://doi.org/10.1007/s00158-016-1455-9.

Sun, X.Z., Shen, B. and Zhang, B.L. (2018), "Experimental study on propagation behavior of three-dimensional cracks influenced by intermediate principal stress", *Geomech. Eng.*, **14**(2), 195-202. https://doi.org/10.12989/gae.2018.14.2.195.

The Shandong Bureau of Coal Mine Security Supervision. (2019), Investigation Report on "11.2" Water and Sand Burst Accident of Yanmei Wanfu Energy Co., Ltd. http://www.sdcoal.gov.cn/channels/ch00196, 2019-02-18.

Tian, W.L. and Yang, S.Q. (2017), "Experimental and numerical study on the fracture coalescence behavior of rock-like materials containing two non-coplanar filled fissures under uniaxial compression", *Geomech. Eng.*, **12**(3), 541-560. https://doi.org/10.12989/gae.2017.12.3.541.

Wang, C., Zhang, S., Zhang, B., Sun, J. and Chen, L. (2020), "Failure characteristics and physical signals of jointed rock: An experimental investigation", *Arab. J. Geosci.*, **13**(14), 1-10. https://doi.org/10.1007/s12517-020-05675-2.

Wu, J., Li, S.C., Xu, Z.H., Pan, D.D. and He, S.J. (2018), "Flow characteristics after water inrush from the working face in karst tunneling", *Geomech. Eng.*, **14**(5), 407-419. https://doi.org/10.12989/gae.2018.14.5.407.

Yu, H.Q. and Xing, W.P. (2014), "Reasons analysis and prevention measures of water bursting from hidden subsided column in Huangcun Branch Coal Mine 10111 working face", *Coal Mine Safety*, **45**(3),183-185.

Zhang, S., Guo, W., Li, Y., Sun, W. and Yin, D. (2017), "Experimental simulation of fault water inrush channel evolution in a coal mine floor", *Mine Water Environ.*, **36**(3), 443-451. https://doi.org/10.1007/s10230-017-0433-9.

Zhang, S., Li, Y., Li, J. Yang, W., Wang, G. and Wen, Z. (2019a), "Experimental studies on variation characteristics of physical parameters during water and sand burst through mining fractures", *J. China Coal Soc*. https://doi.org/10.13225/j.cnki.jccs.2019.0913.

Zhang, S., Shen, B., Li, Y. and Zhou, S. (2019b), "Modeling rock fracture propagation and water inrush mechanisms in underground coal mine", *Geofluids*, (1), 1-15.

Zhao, X., Wang, T., Elsworth, D., He, Y., Zhou, W., Zhuang, L. and Wang, S. (2018), "Controls of natural fractures on the texture of hydraulic fractures in rock", *J. Petrol. Sci. Eng.*, **165**, 616-626. https://doi.org/10.1016/j.petrol.2018.02.047.

Zhou, Z.Q., Li, S.C., Li, L.P., Shi, S.S. and Xu, Z.H. (2015), "An optimal classification method for risk assessment of water inrush in karst tunnels based on grey system theory", *Geomech. Eng.*, **8**(5), 631-647. https://doi.org/10.12989/gae.2015.8.5.631.